Ca^{2+}-dependent induction of TRPM2 currents in hippocampal neurons

Michelle E. Olah[2], Michael F. Jackson[1], Hongbin Li[2], Yaël Perez[3], Hong-Shuo Sun[2,4], Shigeki Kiyonaka[5], Yasuo Mori[5], Michael Tymianski[2,4] and John F. MacDonald[1,2]

[1]*Robarts Research Institute, Molecular Brain Research Group, University of Western Ontario, 100 Perth Drive, London, Ontario, Canada, N6A 5K8*
[2]*Department of Physiology, University of Toronto, 1 King's College Circle, Toronto, Ontario, Canada, M5S 1A8*
[3]*Division of Neurology, Department of Medicine, University of Toronto, Suite RFE 3-805, 190 Elizabeth Street, Toronto, Ontario, Canada, M5G 2C4*
[4]*Toronto Western Hospital Research Institute, 399 Bathurst Street, Toronto, Ontario, Canada, M5T 2S8*
[5]*Laboratory of Molecular Biology, Department of Synthetic Chemistry and Biological Chemistry, Graduate School of Engineering, Kyoto University, Kyoto 615-8510, Japan*

TRPM2 is a Ca^{2+}-permeable member of the transient receptor potential melastatin family of cation channels whose activation by reactive oxygen/nitrogen species (ROS/RNS) and ADP-ribose (ADPR) is linked to cell death. While these channels are broadly expressed in the CNS, the presence of TRPM2 in neurons remains controversial and more specifically, whether they are expressed in neurons of the hippocampus is an open question. With this in mind, we examined whether functional TRPM2 channels are expressed in this neuronal population. Using a combination of molecular and biochemical approaches, we demonstrated the expression of TRPM2 transcripts and proteins in hippocampal pyramidal neurons. Whole-cell voltage-clamp recordings were subsequently carried out to assess the presence of TRPM2-mediated currents. Application of hydrogen peroxide or peroxynitrite to cultured hippocampal pyramidal neurons activated an inward current that was abolished upon removal of extracellular Ca^{2+}, a hallmark of TRPM2 activation. When ADPR (300 μM) was included in the patch pipette, a large inward current developed but only when depolarizing voltage ramps were continuously (1/10 s) applied to the membrane. This current exhibited a linear current–voltage relationship and was sensitive to block by TRPM2 antagonists (i.e. clotrimazole, flufenamic acid and *N*-(*p*-amylcinnamoyl)anthranilic acid (ACA)). The inductive effect of voltage ramps on the ADPR-dependent current required voltage-dependent Ca^{2+} channels (VDCCs) and a rise in $[Ca^{2+}]_i$. Consistent with the need for a rise in $[Ca^{2+}]_i$, activation of NMDA receptors (NMDARs), which are highly permeable to Ca^{2+}, was also permissive for current development. Importantly, given the prominent vulnerability of CA1 neurons to free-radical-induced cell death, we confirmed that, with ADPR in the pipette, a brief application of NMDA could evoke a large inward current in CA1 pyramidal neurons from hippocampal slices that was abolished by the removal of extracellular Ca^{2+}, consistent with TRPM2 activation. Such a current was absent in interneurons of CA1 stratum radiatum. Finally, infection of cultured hippocampal neurons with a TRPM2-specific short hairpin RNA ($shRNA_{TRPM2}$) significantly reduced both the expression of TRPM2 and the amplitude of the ADPR-dependent current. Taken together, these results indicate that hippocampal pyramidal neurons possess functional TRPM2 channels whose activation by ADPR is functionally coupled to VDCCs and NMDARs through a rise in $[Ca^{2+}]_i$

(Received 25 August 2008; accepted after revision 23 December 2008; first published online 5 January 2009)
Corresponding author M. F. Jackson: Robarts Research Institute, Molecular Brain Research Group, University of Western Ontario, 100 Perth Drive, London, ON, Canada, N6A 5K8. Email: mjackson@robarts.ca

TRPM2 forms non-selective cation channels that are stimulated by reactive oxygen/nitrogen species (ROS/RNS) (Hara *et al.* 2002; Wehage *et al.* 2002) through the generation of intracellular ADPR (Perraud *et al.* 2005). ADPR gates TRPM2 channels by binding to the NUDT9H domain of its C-terminus (Perraud *et al.*

M. E. Olah and M. F. Jackson contributed equally to this work.

DOI: 10.1113/jphysiol.2008.162289

2001). In addition to being expressed in peripheral cell types including immunocytes, neutrophils and rat islet cells (Sano *et al.* 2001; Togashi *et al.* 2006; Eisfeld & Luckhoff, 2007), Northern blotting and quantitative PCR techniques indicate that TRPM2 is broadly expressed in the CNS (Nagamine *et al.* 1998; Hara *et al.* 2002; Fonfria *et al.* 2006). However, as this evidence was derived from homogenized tissue samples, it does not allow expression in neurons to be distinguished from that in glia. The importance of making such a distinction is highlighted by a recent study that failed to identify TRPM2 transcripts or functional channels in cerebellar granule cells and astrocytes (Kraft *et al.* 2004). Rather, TRPM2 was detected in microglial cells leading to the suggestion that the CNS distribution of TRPM2 corresponds to its expression in non-neuronal cells (Perraud *et al.* 2003; Kraft & Harteneck, 2005).

Attempts at functionally identifying TRPM2 channels in neurons are hindered by the absence of selective antagonists or blockers. While the blockers characterized to date (e.g. clotrimazole and flufenamic acid) have proven useful in characterizing TRPM2 currents in non-excitable cells, their use in neurons proves more problematic as numerous voltage- and ligand-gated conductances can be blocked as well by these same pharmacological agents. Despite these limitations and contrary to the previous report failing to observe TRPM2 in cerebellar granule cells, there are several lines of evidence that TRPM2 channels are likely expressed in neurons, at least within discrete neuronal populations. For example, TRPM2-like currents have been identified in cultured striatal neurons (Smith *et al.* 2003; Hill *et al.* 2006) as well as in acutely isolated cortical neurons (Kaneko *et al.* 2006). Thus, the issue of whether TRPM2 channels are functionally expressed in central neurons remains controversial and whether or not they are expressed in the principal neurons of the hippocampus remains an open question.

Given the identification of TRPM2 channels as potential mediators of cell death and the selective vulnerability of CA1 pyramidal neurons to ischaemia-induced cell damage, we sought to determine whether functional TRPM2 channels are expressed within this neuronal subpopulation. In the absence of selective blockers, we rely upon a correlative comparison with the biophysical and pharmacological properties of recombinant TRPM2 expressed in various cell lines. We supplement such an approach with molecular, biochemical and cellular techniques to demonstrate that TRPM2 channels are highly expressed in hippocampal pyramidal neurons and that with appropriate stimulation can generate substantive non-selective cation currents. In addition, we demonstrate the functional expression of TRPM2 in CA1 pyramidal cells but not in stratum radiatum interneurons – results that may partially explain the differential sensitivity of these neuronal populations to ischaemia-induced cell death.

Methods

Cell culture

Primary cultures of mouse hippocampal neurons were prepared as previously described (MacDonald *et al.* 1989). Briefly, fetuses were rapidly removed from pregnant (E17–18) Swiss mice under anaesthesia (isoflurane). Hippocampal tissue was dissected and placed in cold Hanks' solution prior to mechanical dissociation by trituration. Cells were plated at a density of $< 1 \times 10^6$ cells ml^{-1} on either 35 mm collagen-coated culture dishes (used for electrophysiological recordings 18–30 days *in vitro* (DIV)) or poly D-lysine-coated 25 mm glass coverslips (used for immunofluorescence 14 DIV) and maintained in serum. All experiments were carried out according to guidelines stipulated by the University of Toronto Animal Care Committee.

Whole-cell recordings from cultured neurons

Whole-cell voltage-clamp recordings were performed at room temperature (20–22°C) using either a Multiclamp 700A or Axopatch-1D amplifier (Molecular Devices, Sunnyvale, CA, USA). Patch electrodes were constructed using a Narishige two-stage puller (PP-83; Narishige, Greenvale, NY, USA) from thin-walled borosilicate glass (TW150-F3; WPI, Sarasota, FL, USA) and input resistance monitored by applying a −10 mV voltage step. Electrodes had a final resistance of 3–5 MΩ when filled with intracellular solution (ICS) containing (in mM): 140 caesium gluconate, 10 Hepes, 2 $MgCl_2$, 0–3 ADPR, pH 7.3 (adjusted with CsOH) and osmolarity between 295 and 300 mosmol l^{-1}. Standard extracellular solution (ECS) was composed of (in mM): 140 NaCl, 5.4 KCl, 25 Hepes, 33 glucose, 2 $CaCl_2$, 1 $MgCl_2$, 0.2 μM TTX, pH of 7.4 (adjusted with NaOH) and osmolarity between 305 and 315 mosmol l^{-1}. $CaCl_2$ was omitted and replaced with 2 mM $BaCl_2$ during segments of some recordings, as indicated in the text. For experiments requiring NMDAR activation, $MgCl_2$ was omitted and 3 μM D-serine, ± 100 μM NMDA added to the standard ECS. Neurons were voltage-clamped at −60 mV and a stream of ECS applied using a computer-controlled, multibarrelled perfusion system (SF-77B; Warner Institute, Hamden, CT, USA) to achieve rapid exchange of solutions (τ of exchange ∼2 ms). Peroxynitrite ($ONOO^-$, Calbiochem)-evoked currents were recorded using solutions prepared under the following conditions. $ONOO^-$ was thawed rapidly and dispensed into aliquots. Tubes were purged with 100% nitrogen gas and frozen and stored at < -70°C.

Aliquots were thawed immediately prior to use and added to ECS that had been vacuum-evacuated of air to enhance $ONOO^-$ solubility and reduce its oxygen-dependent breakdown. $ONOO^-$-containing ECS was prepared immediately prior to each recording. All $ONOO^-$-containing solutions were protected from light. ADPR-dependent currents were induced by the application of a voltage-ramp (±100 mV, 500 ms) to the membrane every 10 s. Current–voltage (*I–V*) relationships were either constructed from these data or from steady-state voltage steps recorded using the following protocol: 0.3 mM ADPR was included in the patch pipette and voltage steps (−80 to +40 mV, 1 s) applied to the membrane every 60 s immediately following both breakthrough and activation of the NMDA-mediated current. All data were filtered at 2 kHz, digitized, and acquired using pCLAMP (Molecular Devices).

Hippocampal slice recordings

Male Sprague–Dawley rats, 6–8 weeks old, were anaesthetized with isoflurane, decapitated and their brains rapidly excised. Transverse hippocampal slices were prepared and placed in a holding chamber for at least 1 h prior to recording. In one set of experiments, a single slice was pretreated with 100 μM NMDA for 5 min and then transferred to a recording chamber and superfused with artificial cerebrospinal fluid (ACSF, 2 ml min^{-1}) composed of (in mM): 124 NaCl, 3 KCl, 1.25 NaH_2PO_4, 1.3 $MgCl_2$, 2.6 $CaCl_2$, 26 $NaHCO_3$, 10 glucose and 0.01 bicuculline methiodide, saturated with 95% O_2–5% CO_2 at 28–30°C. The patch pipette (4–6 MΩ) solution contained (in mM) 132.5 potassium gluconate, 17.5 KCl, 10 Hepes, 0.2 EGTA, 5 QX 314, and 1 ADPR (pH 7.25, 290 mosmol l^{-1}). Patch recordings were done using the 'blind' patch method. Cells were voltage clamped at −20 mV, and experiments started only after the access resistance had stabilized. To activate the ADPR current, voltage-ramps (±100 mV, 500 ms) were applied continuously every 10 s throughout the recording. In a second set of experiments, slices were transferred to the recording chamber and continuously perfused with ACSF (solution as above) at 8 ml min^{-1} without pretreatment in NMDA. Visually guided patch recordings were obtained from CA1 pyramidal cells and visually identified interneurons in stratum radiatum. Patch pipettes contained a solution of (in mM) 150 caesium gluconate, 10 Hepes, 10 $MgCl_2$, 4 Mg-ATP and 1 ADPR (4–6 MΩ resistance). Cells were voltage-clamped at −60 mV. ADPR currents were activated by a 2 μl puff of NMDA (100 mM) directly injected into the recording chamber in a stream of ACSF in close proximity to the slice, in combination with 500 ms-long voltage steps to +60 mV applied every 10 s continuously throughout the recordings. Considering the 2 ml volume of the chamber and the flow rate of 8 ml min^{-1}, this technique allowed the rapid application and washout of high concentrations of NMDA locally (minimal estimated final concentration of NMDA of 100 μM). Data were amplified using an Axopatch 1-D or MultiClamp 700A, sampled at 5–10 kHz, and analysed with pclamp6 software (Axon Instruments, Foster City, CA, USA). Series resistance ranged from 10 to 20 MΩ, as estimated from series resistance compensation of current responses to voltage steps of −10 mV. Cells were discarded if the resistance changed by more than 25%.

In situ hybridization

Brains were dissected from anaesthetized 8-week-old B6 mice after perfusion with 4% paraformaldehyde in 0.1 M sodium phosphate buffer, postfixed overnight at 4°C in the same fixative and subsequently dehydrated, embedded in paraffin, sliced at 8 μm, and mounted onto silicon-coated glass slides. The recombinant pBluescript SK(+) plasmid, pBSII-TRPC7–1B, containing the TRPM2 cDNA fragment (1072–2980) was amplified from full-length mouse cDNA (Hara *et al.* 2002), linearized by digesting the *Eco*R I or *Not* I site (on vector) and transcribed using T3 or T7 MAXIscript RNA polymerase (Ambion, Austin, TX, USA) with DIG RNA Labeling Mix (Roche Molecular Biochemicals) for synthesis of the sense or antisense digoxigenin (DIG)-labelled RNA probes. Sections were partially digested by 0.8% pepsin in 0.2 N HCl and acetylated with 0.25% acetic anhydride in 0.1 M triethanolamine (pH 8.0) after de-paraffinization and rehydration. Hybridization was performed for 12–16 h at 50°C with 400 ng ml^{-1} antisense or sense probe in 10 mM Tris-HCl (pH 7.6), 600 mM NaCl, 0.25% SDS, 1 mM EDTA (pH 8.0), 0.02% polyvinylpyrrolidone, 0.02% Ficoll 400, 0.02% bovine serum albumin, 0.2 mg ml^{-1} yeast tRNA, 10% dextran sulphate, and 50% formamide. The sections were washed in 2 × standard sodium citrate (SSC) with 50% formamide at 50°C for 30 min, treated with 10 μg ml^{-1} RNase A in 10 mM Tris-HCl (pH 7.6), 1 mM EDTA (pH 8.0) and 500 mM NaCl to remove free probes and washed at increasingly high stringencies up to a final condition of 0.2 × SSC at 50°C for 20 min.

Washed slides were incubated in 1.5% blocking reagent (Roche Molecular Biochemicals) in 100 mM Tris-HCl (pH 7.5) and 150 mM NaCl (DIG buffer) at room temperature (RT; 21–23°C) for 1 h. Immunochemical detection of the hybridized probes was performed using alkaline phosphatase-conjugated anti-DIG antibody (Roche Molecular Biochemicals) at 500 times dilution in DIG buffer for 60 min. The alkaline phosphatase activity was visualized by 12–16 h incubation with nitro blue tetrazolium/5-bromo-4-chloro-3-indolyl phosphate alkaline phosphatase detection system (Roche Molecular Biochemicals) in 100 mM Tris-HCl (pH 9.5), 50 mM $MgCl_2$ and 100 mM NaCl under light protection.

Reverse transcriptase-polymerase chain reaction (RT-PCR)

After aspirating the cell into the tip of the micropipette, the tip was broken off and the contents expelled into an Eppendorf tube containing lysis buffer (0.5 ml, Stratagene) supplemented with β-mercaptoethanol (as per manufacturer's instructions). The contents from 10 cells were pooled and single-stranded cDNA was generated from the resulting sample by reverse transcription SuperScript II RNase H-reverse transcriptase (Invitrogen, Carlsbad, CA, USA) with oligo(dT) primer (Invitrogen) following the manufacturer's protocol. The PCR was carried out by using 5 μl of cDNA template, 10 $\times$ PCR buffer (5 μl), $MgCl_2$ (3 μl; 25 mM), dNTPs (1 μl; 10 μM), primers (1 μl each; 25 mM), Ampli*Taq* polymerase (0.5 μl; 5 units μl; Applied Biosystems), and DEPC-treated water for a final volume of 50 μl. Primer sequences for TRPM2 were as follows for primer set 1: Fw, 5′-AAGGAACACAGACAATGCCTG, and Rv, 5′-AGGATGGTCTTGTGGTTCGC; for primer set 2: Fw, 5′- ACTGGATCGTGACAACCCTG and Rv, 5′-AGAGCCACATCCTTCTCAGC.

Membrane preparation and Western blotting

Crude membrane fractions were prepared from cultured hippocampal neurons using a protocol modified from Rogers *et al.* (1991). Briefly, cells were washed in ice-cold solubilization buffer (250 mM sucrose, 1 mM EDTA and MINI cocktail (Roche, Mannheim, Germany)) and Dounce homogenized. The homogenate was centrifuged at 800 *g* for 15 min at 4°C. The supernatant was retained, centrifuged at 50 000 *g* for 90 min and the resulting pellet (crude membrane fraction) was dissolved in buffer containing 2% SDS and 100 mM DTT. Samples were heated to 70°C for 5 min, loaded onto 7.5% SDS-PAGE gels and separated by electrophoresis. Proteins were transferred to nitrocellulose membranes, blocked with 5% non-fat dried milk in Tris-buffered saline for 1 h at RT and incubated with anti-mouse TRPM2 rabbit antiserum for 1 h at RT. Membranes were washed three times in Tris-buffered saline with 0.1% Tween-20 and incubated with HRP-conjugated secondary antibody for 1 h. Following a final wash, bound antibodies were visualized via enhanced chemiluminescence.

Immunofluorescence localization

Cultured hippocampal neurons were washed with phosphate-buffered saline (PBS) and fixed in 4% paraformaldehyde + 4% sucrose in PBS at RT for 20 min. Neurons were washed three times with 0.1% Triton X-100 in PBS (PBST) and blocked in PBST containing 10% normal goat serum (NGS) for 1 h at RT. Immunostaining was carried out in PBST + 1% NGS and neurons were double-labelled as follows: rabbit anti-TRPM2-N-terminal (1 : 500, overnight at 4°C; Bethyl Laboratories, Montgomery, TX, USA), wash with PBST, goat anti-rabbit IgG (1 : 800, 1 h at RT; Alexa 568, Molecular Probes), mouse monoclonal anti-PSD-95 (1 : 500, 1 h at RT, ab2723, Abcam, Cambridge, MA, USA), wash with PBST, goat anti-mouse IgG (1 : 800, 1 h at RT; Alexa 488, Molecular Probes). To visualize nuclei, neurons were stained with Hoechst Stain (1: 2000, 20 min, Sigma) and coverslips mounted with Prolong Gold antifade solution (Invitrogen). Fluorescent images were visualized using an Olympus IX81 microscope.

RNA interference

shRNA preparation and neuronal infection. An shRNA sequence targeting TRPM2 (5′-tAACCTTAGCT CATGGATTCCCtcaagagGGGAATCCATGAGCTAAGGT-Ttttttc-3′ corresponding to coding regions 169–189 relative to the first nucleotide of the start codon of murine TRPM2 (GenBank NM_138301)) and a scrambled (control) sequence (5′-tAATTCTCCGAACG-TGTCACGTtcaagagACGTGACACGTTCGGAGAATTttttt tc-3′) were cloned into a pLB lentiviral vector (Addgene plasmid 11619), which expresses shRNA under control of a U6 promoter and green fluorescent protein (GFP) under control of a CMV promoter. Lentiviruses were generated by transiently transfecting the resulting pLB vectors along with packaging vectors pMDLg/pRRE, pRSV-Rev and pMD2.G into HEK 293T cells (from the human embryonic kidney cell line) using Lipofectamine 2000. The medium containing viruses was harvested 40 h following the start of transfection and concentrated using Millipore Centricon Plus-20 filters. The resulting concentrate (50–100 μl) was used to infect cultured hippocampal neurons at 7 DIV. Infected cultures were used for recordings at 21–24 DIV.

Immunostaining. Mouse cultured hippocampal neurons on coverslips were treated with lentivirus $shRNA_{TRPM2}$ and $shRNA_{control}$ was first washed in PBS. The culture neurons were then fixed and cryo-protected in 2.5% sucrose with 4% paraformaldehyde in PBS solution at RT for 20 min. Immunostaining was performed as previously described (Sun *et al.* 2006). In brief, neurons were blocked using 1% bovine serum albumin, 3% goat serum, 0.3% Triton X-100 in PBS solution for 90 min at RT, and double labelled with rabbit anti-TRPM2 antibody (1 : 50; Abcam), and mouse anti-NeuN antibody (1 : 100; Chemicon, Temecula, CA, USA) overnight at 4°C (gently rocking). Neurons were

subsequently washed with PBS and blocked briefly with the blocking solution. They were incubated with goat anti-rabbit Alexa 568 (1 : 100, Molecular Probes), and goat anti-mouse Alexa 350 (1 : 100; Molecular Probes) for 1 h at RT. After washing, the coverslips were then mounted using ProLong Gold antifade reagent (Invitrogen/Molecular Probes) and viewed with a confocal laser-scanning microscope

Confocal microscopy. Cultured neurons were double-stained with anti-TRPM2 and NeuN antibodies. Triple fluorescence images were visualized with a laser-scanning confocal microscope (Zeiss LSM 510 META) using a $\times 63$ microscope lens (Zeiss). Optical stacks of 5–10 confocal images taken at 0.5 μm intervals were used to generate figures as previously described (Sun *et al.* 2006). (Green represents GFP; red represents anti-TRPM2; blue represents anti-NeuN staining.)

Quantification and statistics. Uninfected neurons (WT, no GFP) from the same fields from the TRPM2-staining images were used as controls, four groups of the cells to compare the fluorescence signals (WT and scrambled shRNA, and WT and TRPM2 shRNA groups). The fluorescence intensities from neuronal cell bodies labelled with TRPM2 and NeuN antibodies were measured using NIH Image J and expressed as arbitrary units (A.U.). Data are presented as mean $\pm$ S.E.M. Group data were compared using one-way ANOVA and multiple comparison test, Fisher LSD test (SigmaStat3.0 of SPSS, Chicago, IL, USA). For all tests, $P < 0.05$ was considered significant.

Results

TRPM2 mRNA and protein are expressed in hippocampal neurons

To determine if TRPM2 is expressed in hippocampal pyramidal neurons, we first employed *in situ* hybridization to examine the distribution of TRPM2 transcripts in mouse sagittal brain sections (Fig. 1*A* and expanded inset). TRPM2 mRNA was broadly distributed with high signal intensities detected within both hippocampal pyramidal and granule neuronal cell layers, a distribution profile suggestive of neuronal expression. To obtain more definitive evidence of specific neuronal expression, patch pipettes were used to aspirate the cytoplasm from visually identified cultured hippocampal neurons. These neurons were selected from a subset of recordings presented below. The resulting samples were pooled and subjected to RT-PCR analysis. Using two distinct primer sets targeted to non-overlapping regions of TRPM2 mRNA, we identified amplified products of the expected size (Fig. 1*B*). In addition, the identity of one of the products was confirmed by DNA sequencing (not shown).

Next, we examined TRPM2 protein expression in a membrane-enriched preparation of cultured hippocampal neurons. Consistent with its predicted size, Western blot analysis revealed the presence of a band of approximately 170 kDa in samples prepared from cultured hippocampal neurons (Fig. 1*C*). One caveat to this result is that neuronal-enriched cultures may also contain other cell types (e.g. fibroblasts and glia), which could contribute to the signal detected on Westerns

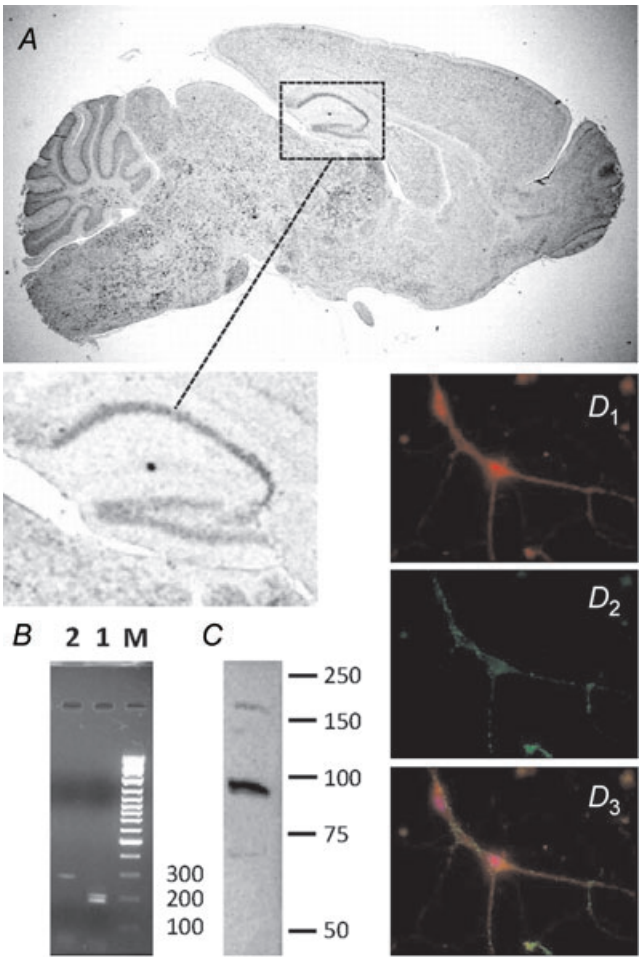

Figure 1. Expression and localization of TRPM2 in mouse brain
A, immunochemical *in situ* hybridization for TRPM2 in sagittal, adult brain slice. Expanded region illustrates presence of hybridization in hippocampal cell layers. *B*, RT-PCR of TRPM2 using distinct primer sets (1 and 2) amplifying non-overlapping regions. *C*, Western blot analysis of TRPM2 expression in crude membrane fraction. *D*, subcellular localization of TRPM2 by immunofluorescence staining in cultured hippocampal neurons: D_1, anti-TRPM2 (red); D_2, anti-PSD-95 (green); D_3, overlay of D_1 and D_2 including visualization of Hoechst nuclear stain (blue).

To confirm the specific expression of TRPM2 protein in neurons and to begin to examine its subcellular distribution, we performed immunostaining using an antibody recognizing the N-terminus of TRPM2 (Zhang *et al.* 2003). TRPM2 immunoreactivity was widely distributed throughout both cell bodies and processes of visually identified pyramidal neurons. TRPM2 staining was diffuse and failed to co-localize preferentially with the synaptic marker, PSD-95 (Fig. 1$D_{1\text{-}3}$). Although we cannot exclude the possibility that TRPM2 is present in excitatory synapses, these data suggest that TRPM2 is not uniquely found in these regions.

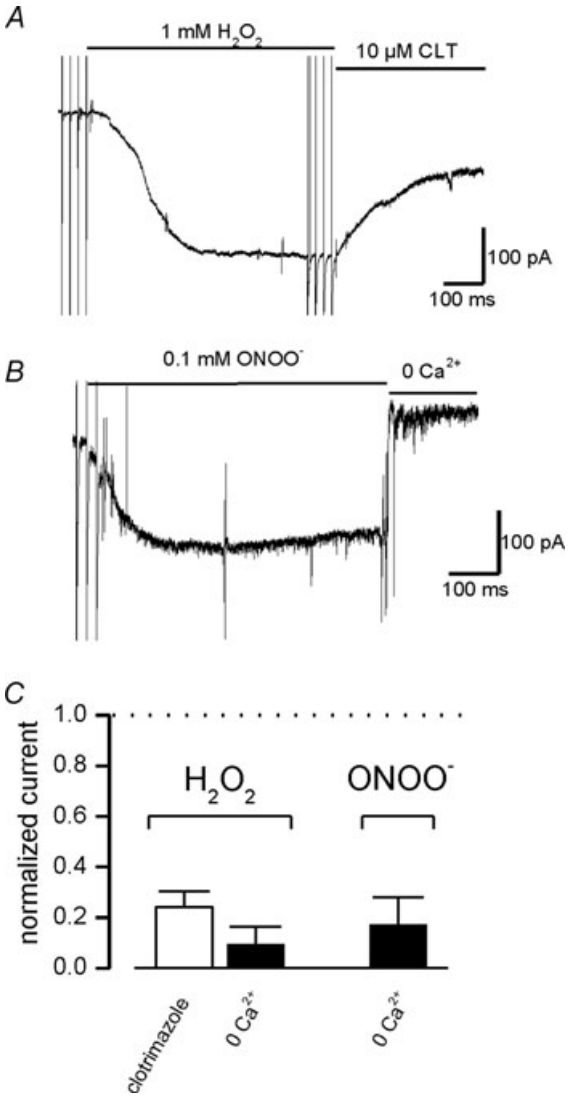

Figure 2. Reactive species activate a TRPM2-like current in cultured hippocampal neurons
A, representative whole-cell recording demonstrating activation of a TRPM2-like current upon extracellular H_2O_2 (1 mM) application and block by CLT (10 μM). Bar indicates period of H_2O_2 or CLT application. *B*, inward current recorded from a single neuron in response to extracellular $ONOO^-$ (0.1 mM) application. *C*, summary bar graph displaying the mean normalized amplitude of the H_2O_2 and $ONOO^-$ current remaining after removal of extracellular Ca^{2+} (H_2O_2, $n = 8$; $ONOO^-$, $n = 6$ or 7) or addition of clotrimazole (CLT) (10 μM) to the ECF (H_2O_2, $n = 9$).

ROS/RNS activate TRPM2-like currents in cultured hippocampal neurons

To begin to examine whether hippocampal neurons possess functional TRPM2 channels, we applied H_2O_2 to voltage-clamped neurons ($V_h = -60$ mV) and monitored changes in the holding current. H_2O_2 (1 mM) induced the development of a large inward current that reached a steady-state amplitude (-198.7 ± 40.23 pA, $n = 8$) within several minutes. The current was then maintained at this level for the remainder of the application period (Fig. 2*A*). The H_2O_2-evoked current was inhibited by application of the TRPM2 antagonist clotrimazole (10 μM) (Hill *et al.* 2004) (-38.3 ± 22.75 pA, $n = 9$) and was abolished by the removal of extracellular Ca^{2+} (24.77 ± 38.59 pA, $n = 8$), previously shown to cause rapid inactivation of TRPM2-mediated currents (Kraft & Harteneck, 2005; Scharenberg, 2005; Eisfeld & Luckhoff, 2007) (Fig. 2*C*).

In addition to ROS, TRPM2 can be activated by select RNS-generating agents (Hara *et al.* 2002). Among nitrogen species generated during oxygen–glucose deprivation of cultured neurons, peroxynitrite ($ONOO^-$), generated through NMDAR-dependent stimulation of nitric oxide synthase, is especially toxic to neurons. Consequently, it was of interest to examine whether $ONOO^-$ could also induce TRPM2-like currents in neurons. Application of $ONOO^-$ (0.1 mM) to cultured hippocampal neurons activated inward currents (-88.8 ± 15.7 pA, $n = 7$), which were inhibited by removal of extracellular Ca^{2+} (10.2 ± 24.1 pA, $n = 6$) (Fig. 2*B* and *C*).

ADPR alone is insufficient to activate TRPM2 in neurons

Though the sensitivity of hippocampal neurons to ROS/RNS is suggestive, the hallmark of TRPM2 channel expression is the activation of large inward currents by intracellularly applied ADPR (Perraud *et al.* 2001; Sano *et al.* 2001; Hara *et al.* 2002). We therefore examined the effects of including ADPR in our patch pipette solution when recording from cultured hippocampal neurons. Intracellular calcium buffering was not used in these recordings. Under these conditions, little or no inward current was observed with intracellular application of ADPR (300 μM or supramaximal concentrations of 1 mM) (data not shown). This is in contrast to reports of recombinant TRPM2 channel activation in HEK 293 cells where the threshold and saturating concentrations of ADPR were 60–100 and 300 μM, respectively (Perraud *et al.* 2001). However, we noted that when we applied

a series of voltage-ramps to monitor changes in the *I–V* relationship, robust inward currents developed in recordings with added ADPR (300 μM, $t = 10$ min: -1221.8 ± 153.7 pA, $n = 12$) but not in those without (-227.7 ± 33.2 pA, $n = 11$) (Fig. 3*A* and *B*). Under the conditions of our recordings, the *I–V* curves generated by applied voltage-ramps were contributed by the sum total of voltage-dependent and resting conductances. At the start of recordings (Fig. 3*C*, trace 1), *I–V* curves showed moderate outward rectification and reversed at negative potentials, reflecting a predominant contribution by resting K^+ conductances. The development of the ADPR-dependent current (Fig. 3*C*, trace 2) was associated with an increase in membrane current (both inward and outward), a pronounced depolarizing shift in the reversal potential of the *I–V* curve (reversal after TRPM2 activation: -21.2 ± 1.7 mV, $n = 11$), and reduction of outward rectification. Subtraction of the ramp generated at the start of recording from that recorded after 10 min of recording (Fig. 3*C*, trace 2–1) revealed the current component recruited by ADPR. The resulting *I–V* curve was linear and reversed at 0 mV, consistent with the reported properties of TRPM2. Since TRPM2 currents are stable and long lasting, we also determined the reversal of *I–V* curves after TRPM2 activation using voltage steps instead of ramps. The reversal under these conditions was identical (-24.1 ± 2.6 mV, $n = 5$).

To confirm the specific expression of ADPR-dependent currents in CA1 pyramidal neurons, we recorded from the CA1 region of acutely prepared hippocampal slices. When voltage-ramps were applied to the membrane as previously described, inclusion of 1 mM ADPR in the patch pipette resulted in the generation of an inward current (Fig. 4*A*). This was associated with the development of a linear *I–V* relationship and a depolarizing shift in the reversal potential to 0 mV, again consistent with properties of TRPM2. Inclusion of 10 μM clotrimazole in the ECS reduced the current amplitude and left-shifted the reversal potential towards resting values (Fig. 4*B* and *C*). In an additional series of recordings from visually identified neurons in hippocampal slices, we compared the amplitude of the ADPR-dependent current in pyramidal neurons and stratum radiatum interneurons of the CA1 region. In this instance, the ADPR-dependent current was induced by a brief application of NMDA to the bath in combination with depolarizing steps to +60 mV every 10 s. In recordings in which 1 mM ADPR was included in the patch pipette, the brief pulse of NMDA provoked the development of a large inward current in pyramidal neurons that was abolished by the removal of extracellular Ca^{2+} (in pA ± S.E.M., -607 ± 142 *versus* -111 ± 28). This current was absent in interneurons (-143 ± 30 *versus* -169 ± 34; Fig. 4*D*).

To explore the relation between applied voltage-ramps and the development of the ADPR-dependent current further, we delayed the start of applied voltage-ramps until 10 min after the beginning of recordings with or without added ADPR. In these recordings, the generation of ADPR-dependent inward currents was delayed until after the start of applied voltage-ramps ($t = 10$ min: -369.1 ± 34.2 pA, $n = 12$; $t = 15$ min: -822.7 ± 178.3 pA, $n = 12$) (Fig. 5*A*). These experiments demonstrate that the application of voltage-ramps provides neurons with an additional stimulus that greatly increases the reliability of generating ADPR-evoked currents in hippocampal neurons.

TRPM2 channel pharmacology

We next explored the pharmacology of the ADPR-dependent currents evoked by voltage-ramps to confirm

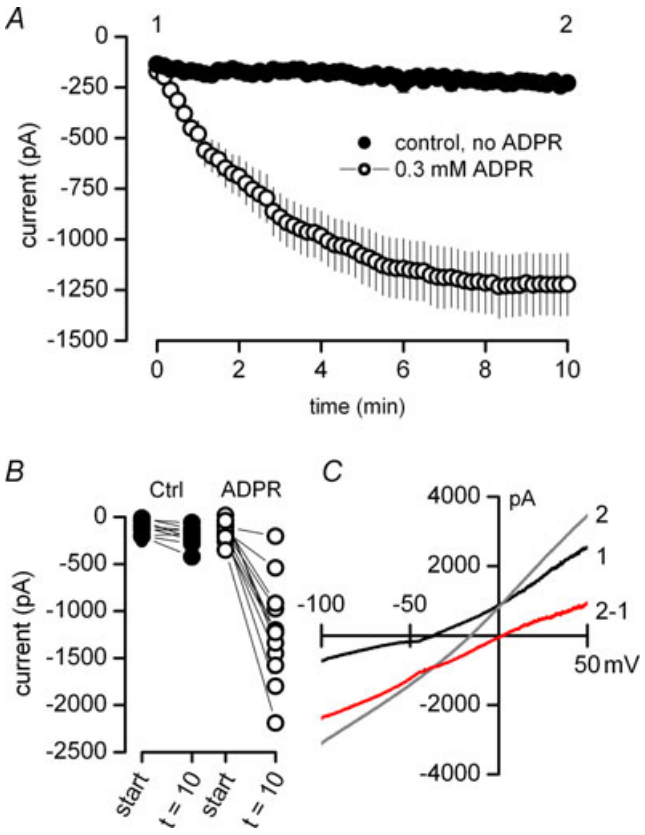

Figure 3. ADP-ribose (ADPR)-dependent currents in cultured hippocampal neurons
A, averaged data illustrates the time course for the development of inward currents in recordings with ADPR added to the patch pipette ($n = 12$). In contrast, the holding current necessary to maintain neurons at −60 mV was unchanged in recordings without added ADPR (control, no ADPR, $n = 11$). *B*, holding current at start of recordings and after 10 min is shown for each individual recording from each of the recording groups. *C*, *I–V* curves from a recording in which ADPR was added to the patch pipette. Traces were taken from voltage-ramps applied at the start of recording (trace 1) and after 10 min (trace 2). The specific contribution from the ADPR-dependent current was derived by subtracting the *I–V* curve generated at the start from that which was recorded at 10 min (trace 2–1).

that these are in fact mediated by TRPM2. Recombinant TRPM2 currents are blocked by a series of compounds including clotrimazole, ACA and flufenamic acid (Harteneck *et al.* 2007). In addition, TRPM2 currents can be inactivated by the removal of extracellular Ca^{2+} (Hara *et al.* 2002). In contrast, TRPM2 currents are either insensitive or enhanced by extracellular application of La^{3+} (Kraft *et al.* 2004), an effective blocker of many non-selective cation channels including several other members of the TRP family of ion channels (Kraft & Harteneck, 2005). In the absence of TRPM2-selective antagonists, we therefore tested each of these blockers on the ADPR-dependent current in hippocampal neurons. As illustrated by the series of representative *I–V* curves, removal of extracellular Ca^{2+} (Fig. 6*A* and *B*) as well as application of either clotrimazole (Fig. 6*A* and *C*), flufenamic acid (Fig. 6*A* and *D*) or ACA (Fig. 6*A* and *E*) depressed the ADPR-induced current and shifted the reversal potential of *I–V* curves back towards their initial, more negative value. In contrast, application of La^{3+} enhanced the ADPR-dependent current (Fig. 6*A* and *F*). The resulting pharmacological profile is entirely consistent with the activation of TRPM2 channels in hippocampal culture neurons.

Ca^{2+} dependence of ADPR-activated current

While recombinant TRPM2 channels are sensitive to the removal of extracellular Ca^{2+}, this effect is ultimately mediated by the action of Ca^{2+} at an intracellular site located on either the channel or a closely associated protein (McHugh *et al.* 2003). We therefore examined whether the voltage-ramp-mediated activation of ADPR-dependent currents in hippocampal neurons required an elevation of intracellular Ca^{2+}. The intracellular buffering capacity in our recordings was raised by adding 20 mM BAPTA to our ADPR-containing ICS. Under these conditions, intracellular Ca^{2+} was buffered to an estimated final concentration of 100 nM. Using the same ramp protocol as in previous experiments, buffering intracellular Ca^{2+} to 100 nM suppressed the induction of TRPM2-like currents in cultured hippocampal neurons (ADPR alone: -477.1 ± 97.6 pA,

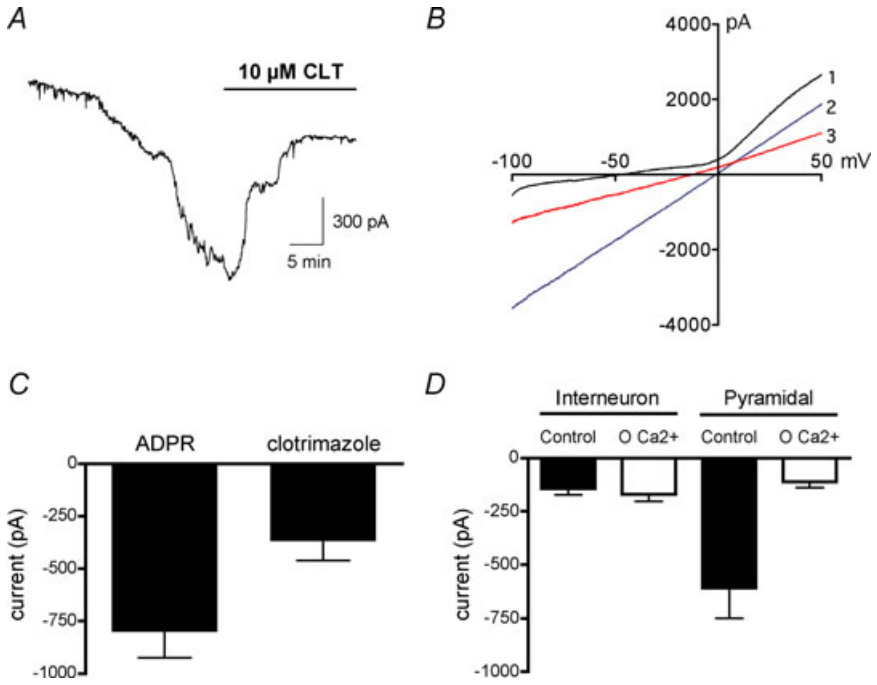

Figure 4. Activation of the ADPR-dependent current in hippocampal slices in CA1 pyramidal neurons but not in stratum radiatum interneurons
A, representative whole-cell recording from a CA1 pyramidal neuron demonstrating activation of an ADPR-dependent current (1 mM ADPR in the patch pipette). The amplitude of the current was reduced by extracellular application of 10 μM clotrimazole (CLT) as shown. Ramps were blanked for clarity. *B*, *I–V* curves from the same cell. Traces were taken from voltage-ramps applied at the start of recording (trace 1), after 30 min (trace 2) and following perfusion of the slice for 20 min with ACSF containing 10 μM CLT (trace 3). *C*, summary bar graph demonstrating inhibition of ADPR-dependent current by 10 μM CLT ($n = 4$). *D*, summary bar graph of ADPR-dependent currents induced by application of NMDA and abolished by removal of extracellular Ca^{2+} in CA1 pyramidal cells ($n = 6$ and 8) and stratum radiatum interneurons ($n = 7$ and 6).

$n = 13$; ADPR + BAPTA: -265.0 ± 27.9 pA, $n = 10$) (Fig. 5*B*).

We therefore suspected that the observed dependence of TRPM2-like currents on voltage-ramps was due to Ca^{2+} entry via recruitment of VDCCs. To examine the involvement of VDCCs, we tested the effects of co-applied Cd^{2+} (100 μM) and Ni^{2+} (100 μM), two broad-spectrum VDCC blockers (Fox *et al.* 1987), on the ability of voltage-ramps to promote the generation of ADPR-dependent current (300 μM). Blocking VDCCs completely eliminated the induction of the ADPR-dependent current by voltage-ramps in cultured hippocampal neurons (-85.0 ± 16.0 pA, $n = 6$) (Fig. 5*B*).

Our results demonstrate, that in addition to ADPR, the gating of TRPM2-like currents in cultured hippocampal neurons requires a rise in intracellular Ca^{2+}, as resting levels are insufficient to support channel activation. This is in contrast to findings in recombinant cell systems where the intracellular application of ADPR alone is sufficient to activate TRPM2. The influx of extracellular Ca^{2+} through activated VDCCs accounts for one source of increased $[Ca^{2+}]_i$. We therefore examined whether TRPM2-like channel activation specifically required VDCCs or whether other routes of Ca^{2+} entry could also activate these channels. Since NMDARs serve as a major Ca^{2+} influx pathway in hippocampal neurons and their over-activation leads to excitotoxic cell death, we tested whether stimulation of NMDARS could activate the ADPR-dependent current.

As expected, in the absence of NMDA application, no increase in holding current was observed when 300 μM ADPR was included in the patch pipette (not shown). However, brief, repeated NMDA applications (100 μM for 5 s every 2 min) induced a large ADPR-dependent current (-1221.0 ± 132.0 pA, $n = 16$, Fig. 5*B*).

shRNA knockdown of TRPM2

In order to further substantiate the participation of TRPM2 channels to the ADPR-dependent current, we used short hairpin RNA (shRNA)-mediated gene silencing to reduce the expression levels of TRPM2 in our cultured neurons. Several sequences were first screened in HEK 293 cells expressing TRPM2. We identified a specific sequence ($shRNA_{TRPM2}$) that could substantially reduce ADPR-evoked current amplitudes in these cells (not shown). A scrambled shRNA sequence was used as control ($shRNA_{scrambled}$).

Given the difficulty of achieving high efficiency transfection of post-mitotic cells such as neurons, $shRNA_{TRPM2}$ and $shRNA_{scrambled}$ were cloned into a lentiviral vector that also allowed for expression of GFP. Visual inspection of GFP expression confirmed that high infection rates (> 80%) were achieved in our cultured hippocampal neurons with both $shRNA_{TRPM2}$ and $shRNA_{control}$ lentiviruses. We first confirmed the ability of $shRNA_{TRPM2}$ to reduce the expression of TRPM2 in infected cultures by quantifying the intensity of TRPM2 immunostaining (Fig. 7). This staining was compared both between infected (GFP positive) and non-infected (GFP negative, wild-type (WT)) neurons within each culture dish and between cultures expressing either $shRNA_{TRPM2}$ or $shRNA_{control}$. As an internal negative control, we also compared the intensity of NeuN (Fig. 7*D*) under identical conditions. In neurons expressing $shRNA_{TRPM2}$, TRPM2 expression was reduced by ~45% compared to neurons expressing $shRNA_{control}$ ($shRNA_{TRPM2} = 125.3 \pm 9$; $shRNA_{control} = 222.8 \pm 5.7$) whereas no difference was observed between $shRNA_{control}$-expressing neurons and uninfected WT

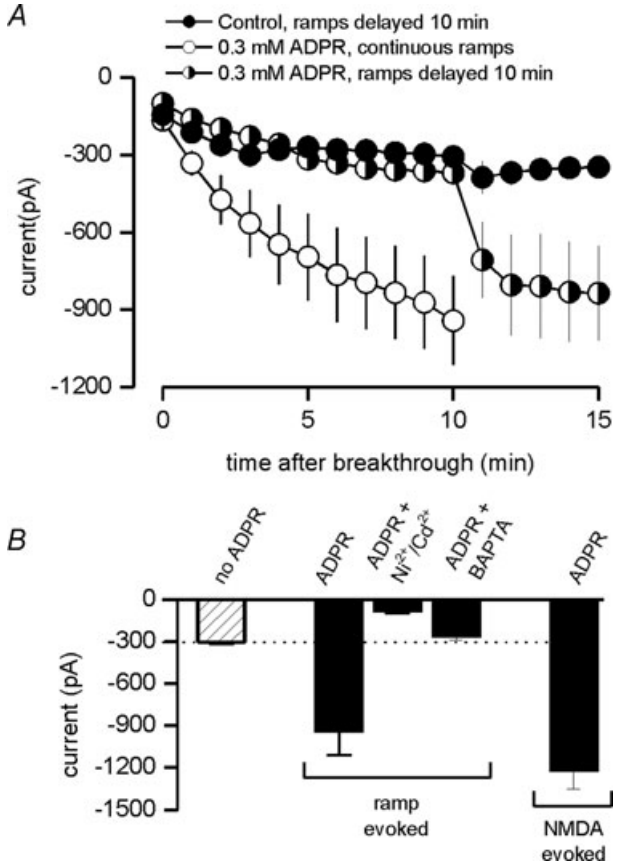

Figure 5. Applied voltage-ramps are necessary for the induction of ADPR-dependent currents
A, average whole-cell currents recorded from neurons with or without added ADPR and in which voltage-ramps were applied continuously or delayed for 10 min. *B*, summary bar graph illustrating the effects of the various indicated treatments on the amplitude of the ADPR-dependent current measured 10 min after the start of recordings for ramp-induced and 16 min for NMDA-induced. No ADPR ($n = 5$); ramps: ADPR ($n = 13$), ADPR + Ni^{2+}/Cd^{2+} ($n = 6$), ADPR + BAPTA ($n = 10$); NMDA: ADPR ($n = 16$).

neurons (Fig. 7*A*, *B* and *C*). In contrast, no difference was observed in NeuN staining between the various treatment groups (Fig. 7*A*, *B* and *D*). We also observed no difference in the relative GFP intensity between $shRNA_{control}$ and $shRNA_{TRPM2}$-expressing neurons ($shRNA_{TRPM2} = 227.9 \pm 1.0$; $shRNA_{control} = 234.0 \pm 0.9$, not shown).

Having confirmed the effectiveness of $shRNA_{TRPM2}$ at reducing the expression of TRPM2, we attempted to record ADPR-dependent currents in visually identified GFP-positive neurons from cultures infected with either $shRNA_{TRPM2}$ or $shRNA_{scrambled}$ lentiviruses. In these experiments, NMDA applications were used to activate the ADPR-dependent current. In this way, the amplitude of

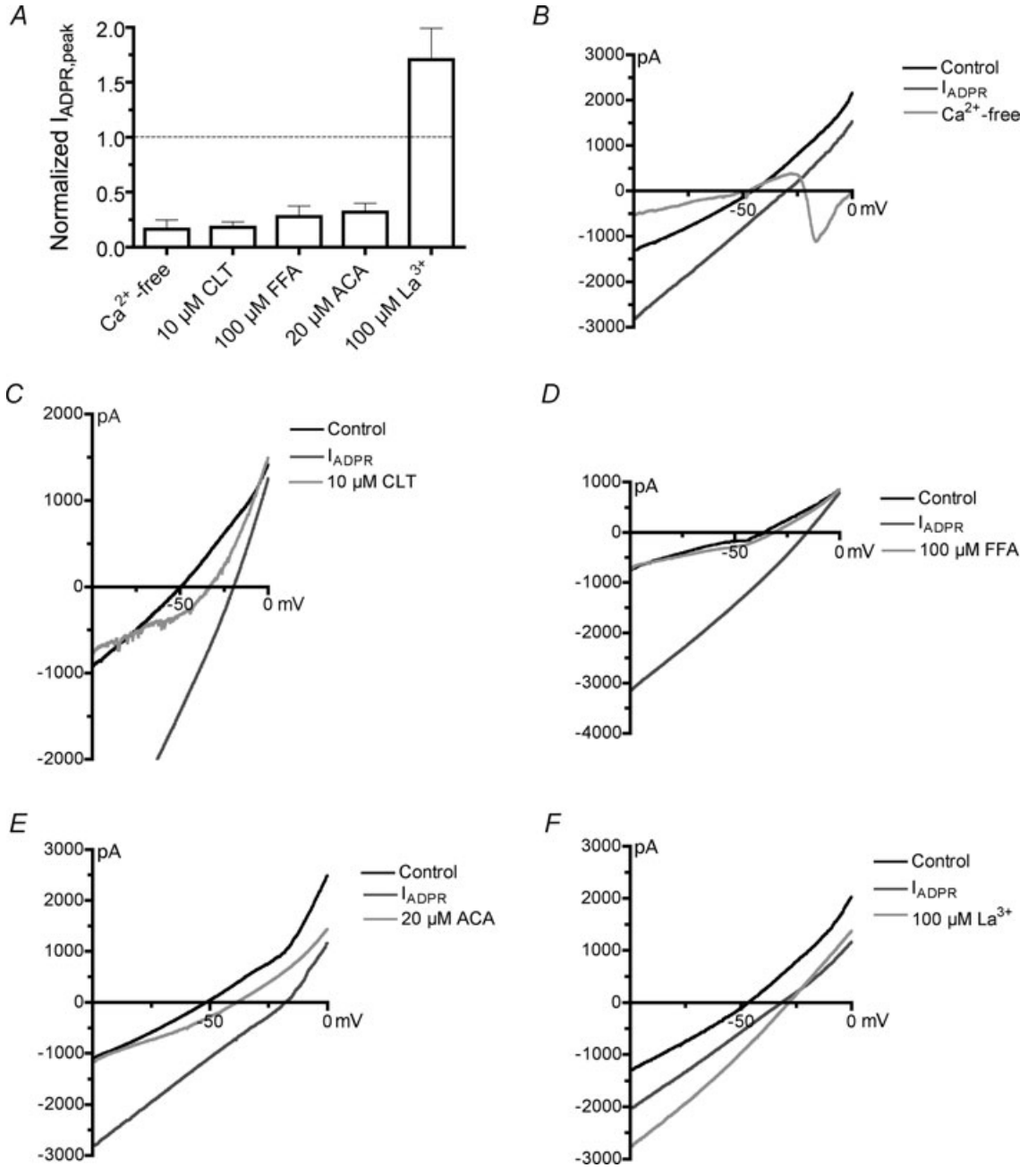

Figure 6. The pharmacological profile of the ADPR-dependent current in cultured hippocampal neurons matches that of TRPM2

Summary data (*A*) and representative voltage-ramps (*B–F*) of effect of removing extracellular Ca^{2+} (*A* and *B*) or application of either clotrimazole (10 μM) (*A* and *C*), flufenamic acid (100 μM) (*A* and *D*), ACA 20 μM (*A* and *E*) or La^{3+} (100 μM) (*A* and *F*) on the maximal ADPR-dependent current.

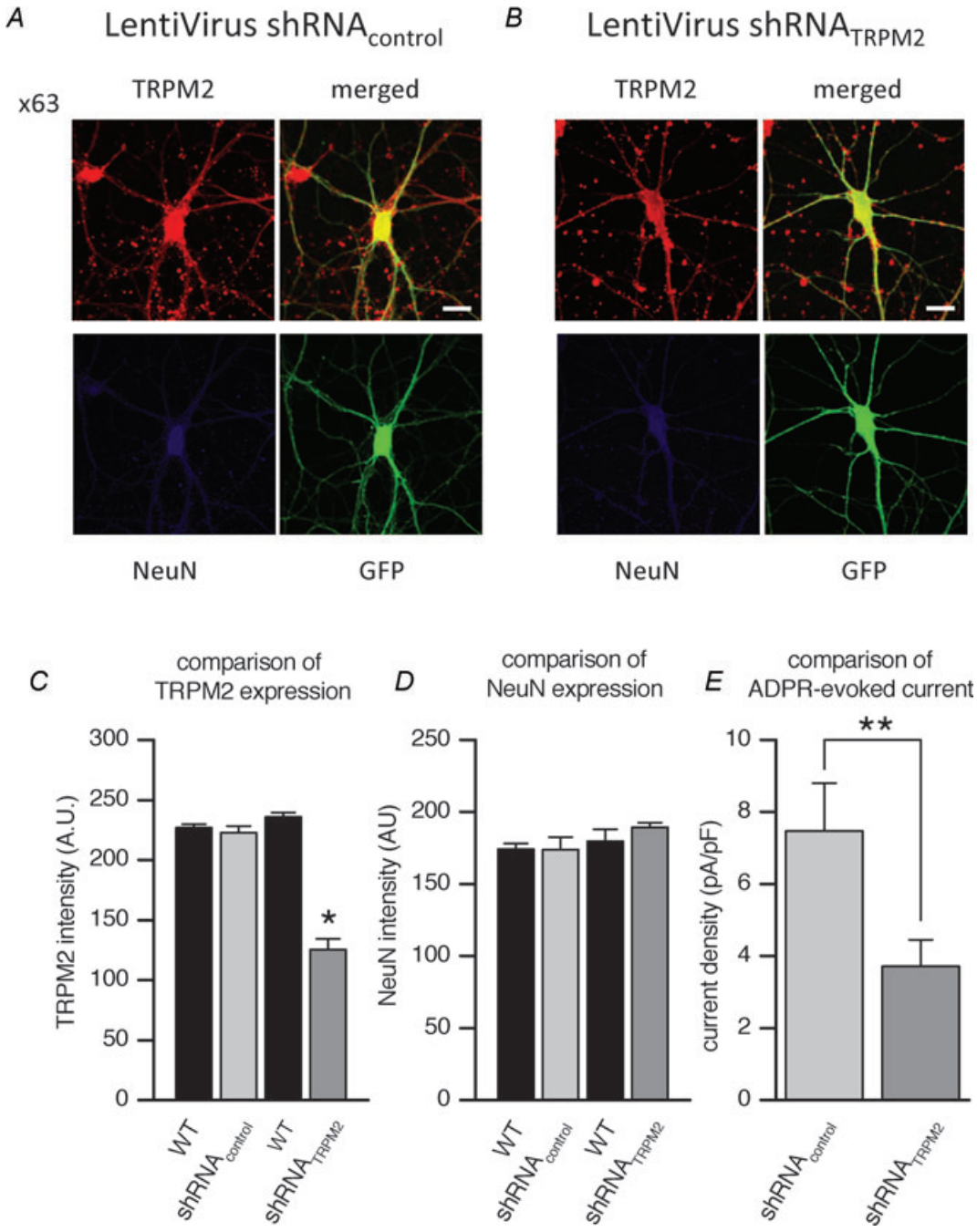

Figure 7. shRNA knockdown of TRPM2 prevents activation of the ADPR-dependent current
A and *B*, confocal images from cultures treated as indicated. High magnification (×63 objective) image of the TRPM2 immunosignal (red) (*A* and *B*, top left) and GFP fluorescence (green) (*A* and *B*, lower right). Anti-NeuN staining (blue) of GFP-positive cells (*A* and *B* lower left). Scale bar = 20 μm. *C*, comparison of fluorescence intensities from cell bodies of WT (uninfected) and neurons infected with $shRNA_{control}$ and $shRNA_{TRPM2}$ ($n = 8$/group). The TRPM2 fluorescence intensity from cell bodies of the $shRNA_{TRPM2}$-treated group is significantly lower than that of the $shRNA_{control}$-treated group (also from that of WT cells (GFP negative) from both treatment groups) as indicated by * (difference, $P < 0.001$, ANOVA; $P < 0.001$, multiple comparison test (Fisher's least significant difference test)). *D*, as a control, the NeuN fluorescence intensity was also quantified and used as reference in all 4 groups for the comparison ($n = 8$/group). No difference in the NeuN expression of these neurons was observed. *E*, comparison of the ADPR-dependent current induced by NMDA application in neurons treated with $shRNA_{TRPM2}$ ($n = 9$) or $shRNA_{control}$ ($n = 7$). The amplitude of the current (normalized to cell capacitance) was determined after 10 min of recordings. The ADPR-dependent current recorded from $shRNA_{TRPM2}$-treated neurons was significantly smaller than in $shRNA_{control}$-treated neurons (**$P < 0.05$, Student's *t* test).

NMDAR-mediated currents could be used as an additional control for potential off-target effects of $shRNA_{TRPM2}$. $shRNA_{TRPM2}$ reduced the amplitude of ADPR-dependent currents (Fig. 7*E*) whilst NMDAR-mediated currents were unchanged (not shown, NMDAR-mediated peak amplitudes: $shRNA_{TRPM2} = -4655.2 \pm 490.9$ pA; $shRNA_{control} = -3894.1 \pm 445.0$ pA, difference was not significant).

Discussion

Intracellular Ca^{2+} homeostasis is controlled in part by three major adenine intracellular second messengers: ADPR, cyclic ADPR (cADPR) and nicotinic acid–adenine dinucleotide phosphate (NAADP) (Harteneck *et al.* 2007). cADPR activates the ryanodine receptor, NAADP may stimulate a novel Ca^{2+} channel (Kraft *et al.* 2004) and ADPR gates Ca^{2+}-permeable TRPM2 channels. Interestingly, each of these messengers is metabolically related, suggesting they may make distinct but coordinated contributions to Ca^{2+} signalling by modulating the gating of their respective target channels. TRPM2 is expressed in diverse cell types and despite convincing evidence for high expression in the mammalian brain, much of this signal was attributed to strong expression in non-neuronal cells. Thus, the existence of functional TRPM2 channels in neurons remains controversial at best. Using cellular, biochemical and molecular approaches we now show that functional TRPM2 channels are highly expressed in pyramidal neurons of the hippocampus, including those of the CA1 region. Conversely, we did not find any functional evidence for TRPM2 expression in a subgroup of CA1 interneurons in hippocampal slices. Moreover, we demonstrate that ADPR alone is insufficient to gate TRPM2 in hippocampal neurons. Rather a concomitant influx of Ca^{2+} through VDCCs or NMDARs is necessary to fully activate TRPM2 channels.

In recombinant systems, applications of ADPR lead to the direct gating of TRPM2 channels, indicating that ADPR is an intracellular TRPM2 agonist. In addition to ADPR, ion substitution experiments aimed at characterizing the cation permeability of TRPM2 channels revealed a role for extracellular Ca^{2+} as a positive regulator of TRPM2 (Hara *et al.* 2002). Subsequently, McHugh *et al.* (2003) demonstrated that the gating of TRPM2 by ADPR was critically dependent on intracellular Ca^{2+}, consistent with earlier suggestive evidence (Perraud *et al.* 2001). However, no evidence that Ca^{2+} can itself directly gate TRPM2 channels exists. Rather, elevated $[Ca^{2+}]_i$ shift the ADPR concentration–effect relationship thereby facilitating activation of TRPM2 by ADPR (Perraud *et al.* 2001; Heiner *et al.* 2006).

In recombinant expression systems, the Ca^{2+} required for ADPR gating may, at least in part, be derived from entry into cells via TRPM2 channels themselves. In this scenario, initial infrequent openings of even a few channels provide a highly localized influx of Ca^{2+}. However, due to the high channel density that exists in these systems, this small initial Ca^{2+} influx is sufficient to facilitate the opening of neighbouring channels, leading to rapid and self-sustained positive feedback. However, Ca^{2+} influx through TRPM2 is insufficient to allow gating by ADPR in endogenous systems where channel density is much lower. Indeed, minimal gating of TRPM2 channels by ADPR occurred in neutrophil granulocytes unless recordings were made using pipette solutions containing high Ca^{2+}, leading to the suggestion that endogenous ADPR 'enables' TRPM2 activation (Kraft & Harteneck, 2005).

Our recordings from cultured hippocampal neurons were carried out in the absence of exogenous intracellular Ca^{2+} buffering in order to promote maximal channel activation. However, even under these conditions, application of supramaximal concentrations (1 mM) of ADPR could not reliably evoke TRPM2 currents on its own; an additional stimulus providing an initial influx of Ca^{2+} was required. This could be achieved in neurons by applying voltage-ramps. The ramp-induction of these currents was prevented by extracellular Ni^{2+} and Cd^{2+} as well as by buffering intracellular Ca^{2+} with BAPTA, confirming the role of Ca^{2+} entry through VDCCs. Therefore, TRPM2 channels in hippocampal neurons require both 'priming' by ADPR as well as 'induction' by Ca^{2+} influx through VDCCs. This requirement may account for the previous report that TRPM2-like currents are exceedingly small in cultured cortical neurons (Kraft *et al.* 2004).

The study of many TRP family channel members is made difficult due to the absence of selective blockers. This is especially true when characterizing these channels in neurons where multiple ligand- and voltage-gated channels can be coincidently activated. We therefore utilized a number of comparative criteria to establish that the voltage-ramp-induced currents were mediated by TRPM2. Firstly, the currents were never observed unless ADPR was included in our intracellular pipette solution. The use of ADPR for the identification of TRPM2 is beneficial in this respect as, to our knowledge, only one other channel can reportedly be activated by ADPR in mammalian cells. A Ca^{2+}-activated K^+ channel expressed in vascular smooth muscle cells is activated by ADPR and mediates K^+ efflux from cells (Li *et al.* 1998). As these currents are outwardly directed, they did not contribute to our inward ADPR-dependent currents. Secondly, our current resembled TRPM2 currents recorded in HEK 293 cells in that both: (a) demonstrated near linear *I–V* curves, (b) had reversal potentials consistent with non-selective cation channels, (c) were suppressed by removing extracellular Ca^{2+}, and (d) required intracellular Ca^{2+} for gating of the channels by

ADPR. Thirdly, the voltage-ramp-activated ADPR-primed currents in cultured neurons were strongly depressed by appropriate concentrations of recombinant TRPM2 channel blockers including clotrimazole, flufenamic acid and ACA. Furthermore, the ADPR-evoked currents were insensitive or even enhanced by applications of La^{3+}, a broad-spectrum blocker of numerous non-selective channels including several TRP family members. Nevertheless, the participation of TRPM2 channels in the ADPR current in hippocampal neurons was further confirmed using a vector-based approach to express an shRNA sequence ($shRNA_{TRPM2}$) that selectively reduced TRPM2 expression. Infection of cultured hippocampal neurons with $shRNA_{TRPM2}$ lentivirus reduced the expression of TRPM2, as revealed by immunostaining, and reduced the amplitude of ADPR currents, in this case evoked by NMDA application. Collectively this pharmacological, biophysical and molecular profile provides strong evidence that functional TRPM2 channels are expressed in hippocampal neurons and that TRPM2 currents can be induced by influx of Ca^{2+} via voltage-dependent Ca^{2+} channels (or NMDARs) provided intracellular ADPR is made available to prime the channels.

In contrast to our findings, Kraft *et al.* (2004) failed to detect TRPM2 in cultured cerebellar granule neurons suggesting instead that TRPM2 was expressed in microglia. Taken together, their findings and ours indicate that, though broadly distributed in the CNS, the particular cell types expressing TRPM2 vary regionally. This in turn suggests that TRPM2 serves distinct regional functions. Given the selective vulnerability of CA1 pyramidal neurons to ischaemic damage (Abe *et al.* 1995), the functional expression of Ca^{2+}-permeable TRPM2 within this neuronal population is noteworthy. Interestingly, the Ca^{2+} to monovalent ion permeability ratio of TRPM2 is comparable to that of NMDARs (Jahr & Stevens, 1993; Wollmuth & Sakmann, 1998; Togashi *et al.* 2008). However, unlike NMDARs, TRPM2 channels are not subject to voltage-dependent block by extracellular Mg^{2+}, suggesting that TRPM2 channels could provide much greater Ca^{2+} entry and correspondingly be more toxic to neurons when active. Indeed, sustained intracellular Ca^{2+} elevation following TRPM2 activation has been causally linked to cell death in a variety of cell types under conditions promoting oxidative and nitrosative stress. Such conditions are well known to exist during experimentally induced oxygen–glucose deprivation. In cultured cortical neurons, oxygen–glucose deprivation leads to the release of glutamate and excessive NMDAR activation (Lipton, 1999). Due to the coupling of NMDARs to NOS via PSD-95, cell death pathways are stimulated in a 'source-specific' manner by Ca^{2+} entry via activated NMDARs (Sattler *et al.* 1999). The resulting activation of NOS leads to accumulation of $ONOO^-$, which proves especially toxic to neurons (Aarts & Tymianski, 2004). Our demonstration that $ONOO^-$ activated TRPM2 channels in pyramidal neurons is thus important in this respect. Importantly, to our knowledge, there is no evidence to suggest that NO may directly activate TRPM2. Any role for NOS in the activation of TRPM2 would therefore strictly be through its contribution to the production of $ONOO^-$. Future studies will be needed to determine whether this can in fact occur.

Finally, when recording from cultured hippocampal neurons, the various pyramidal neurons of the hippocampus (CA1–CA4) cannot be readily distinguished. However, recordings from CA1 pyramidal neurons in slices, including a subset from visually identified neurons, confirm the functional expression of TRPM2 in these neurons, known to be especially vulnerable to ischaemia. In contrast, we could not find evidence for the functional expression of TRPM2 in visually identified interneurons; a neuronal population that is reportedly resistant to this type of insult (Ferrer *et al.* 1995; Inglefield *et al.* 1997; Sugawara *et al.* 2002; Frahm *et al.* 2004). Accordingly, the differential functional expression of TRPM2 channels may partially explain the differential sensitivity of these neuronal populations to ischaemic insults. Similarly, although not present in cerebellar granule cells, it remains of interest to determine whether TRPM2 channels are expressed in Purkinje cells, which, like CA1 hippocampal neurons, are especially vulnerable to ischaemia-induced cell death (Brorson *et al.* 1995). In addition, although *in situ* hybridization would suggest that TRPM2 transcripts are diffusely expressed throughout hippocampal pyramidal subregions (CA1–CA4), additional studies will be needed in order to determine the extent to which TRPM2 is functionally expressed in each of these neuronal populations.

References

Aarts MM & Tymianski M (2004). Molecular mechanisms underlying specificity of excitotoxic signaling in neurons. *Curr Mol Med* **4**, 137–147.

Abe K, Aoki M, Kawagoe J, Yoshida T, Hattori A, Kogure K & Itoyama Y (1995). Ischemic delayed neuronal death. A mitochondrial hypothesis. *Stroke* **26**, 1478–1489.

Brorson JR, Manzolillo PA, Gibbons SJ & Miller RJ (1995). AMPA receptor desensitization predicts the selective vulnerability of cerebellar Purkinje cells to excitotoxicity. *J Neurosci* **15**, 4515–4524.

Eisfeld J & Luckhoff A (2007). TRPM2. *Handb Exp Pharmacol* **179**, 237–252.

Ferrer I, Soriano MA, Vidal A & Planas AM (1995). Survival of parvalbumin-immunoreactive neurons in the gerbil hippocampus following transient forebrain ischemia does not depend on HSP-70 protein induction. *Brain Res* **692**, 41–46.

Fonfria E, Murdock PR, Cusdin FS, Benham CD, Kelsell RE & McNulty S (2006). Tissue distribution profiles of the human TRPM cation channel family. *J Recept Signal Transduct Res* **26**, 159–178.

Fox AP, Nowycky MC & Tsien RW (1987). Kinetic and pharmacological properties distinguishing three types of calcium currents in chick sensory neurones. *J Physiol* **394**, 149–172.

Frahm C, Haupt C & Witte OW (2004). GABA neurons survive focal ischemic injury. *Neuroscience* **127**, 341–346.

Hara Y, Wakamori M, Ishii M, Maeno E, Nishida M, Yoshida T, Yamada H, Shimizu S, Mori E, Kudoh J, Shimizu N, Kurose H, Okada Y, Imoto K & Mori Y (2002). LTRPC2 Ca^{2+}-permeable channel activated by changes in redox status confers susceptibility to cell death. *Mol Cell* **9**, 163–173.

Harteneck C, Frenzel H & Kraft R (2007). *N*-(*p*-amylcinnamoyl) anthranilic acid (ACA): a phospholipase A_2 inhibitor and TRP channel blocker. *Cardiovasc Drug Rev* **25**, 61–75.

Heiner I, Eisfeld J, Warnstedt M, Radukina N, Jungling E & Luckhoff A (2006). Endogenous ADP-ribose enables calcium-regulated cation currents through TRPM2 channels in neutrophil granulocytes. *Biochem J* **398**, 225–232.

Hill K, McNulty S & Randall AD (2004). Inhibition of TRPM2 channels by the antifungal agents clotrimazole and econazole. *Naunyn Schmiedebergs Arch Pharmacol* **370**, 227–237.

Hill K, Tigue NJ, Kelsell RE, Benham CD, McNulty S, Schaefer M & Randall AD (2006). Characterisation of recombinant rat TRPM2 and a TRPM2-like conductance in cultured rat striatal neurones. *Neuropharmacology* **50**, 89–97.

Inglefield JR, Wilson CA & Schwartz-Bloom RD (1997). Effect of transient cerebral ischemia on γ-aminobutyric $acid_A$ receptor α1-subunit-immunoreactive interneurons in the gerbil CA1 hippocampus. *Hippocampus* **7**, 511–523.

Jahr CE & Stevens CF (1993). Calcium permeability of the *N*-methyl-D-aspartate receptor channel in hippocampal neurons in culture. *Proc Natl Acad Sci U S A* **90**, 11573–11577.

Kaneko S, Kawakami S, Hara Y, Wakamori M, Itoh E, Minami T, Takada Y, Kume T, Katsuki H, Mori Y & Akaike A (2006). A critical role of TRPM2 in neuronal cell death by hydrogen peroxide. *J Pharmacol Sci* **101**, 66–76.

Kraft R, Grimm C, Grosse K, Hoffmann A, Sauerbruch S, Kettenmann H, Schultz G & Harteneck C (2004). Hydrogen peroxide and ADP-ribose induce TRPM2-mediated calcium influx and cation currents in microglia. *Am J Physiol Cell Physiol* **286**, C129–C137.

Kraft R & Harteneck C (2005). The mammalian melastatin-related transient receptor potential cation channels: an overview. *Pflugers Arch* **451**, 204–211.

Li PL, Zou AP & Campbell WB (1998). Regulation of KCa-channel activity by cyclic ADP-ribose and ADP-ribose in coronary smooth muscle. *Am J Physiol* **275**, H1002–H1010.

Lipton P (1999). Ischemic cell death in brain neurons. *Physiol Rev* **79**, 1431–1568.

MacDonald JF, Mody I & Salter MW (1989). Regulation of *N*-methyl-D-aspartate receptors revealed by intracellular dialysis of murine neurones in culture. *J Physiol* **414**, 17–34.

McHugh D, Flemming R, Xu SZ, Perraud AL & Beech DJ (2003). Critical intracellular Ca^{2+} dependence of transient receptor potential melastatin 2 (TRPM2) cation channel activation. *J Biol Chem* **278**, 11002–11006.

Nagamine K, Kudoh J, Minoshima S, Kawasaki K, Asakawa S, Ito F & Shimizu N (1998). Molecular cloning of a novel putative Ca^{2+} channel protein (TRPC7) highly expressed in brain. *Genomics* **54**, 124–131.

Perraud AL, Fleig A, Dunn CA, Bagley LA, Launay P, Schmitz C, Stokes AJ, Zhu Q, Bessman MJ, Penner R, Kinet JP & Scharenberg AM (2001). ADP-ribose gating of the calcium-permeable LTRPC2 channel revealed by Nudix motif homology. *Nature* **411**, 595–599.

Perraud AL, Schmitz C & Scharenberg AM (2003). TRPM2 Ca^{2+} permeable cation channels: from gene to biological function. *Cell Calcium* **33**, 519–531.

Perraud AL, Takanishi CL, Shen B, Kang S, Smith MK, Schmitz C, Knowles HM, Ferraris D, Li W, Zhang J, Stoddard BL & Scharenberg AM (2005). Accumulation of free ADP-ribose from mitochondria mediates oxidative stress-induced gating of TRPM2 cation channels. *J Biol Chem* **280**, 6138–6148.

Rogers SW, Hughes TE, Hollmann M, Gasic GP, Deneris ES & Heinemann S (1991). The characterization and localization of the glutamate receptor subunit GluR1 in the rat brain. *J Neurosci* **11**, 2713–2724.

Sano Y, Inamura K, Miyake A, Mochizuki S, Yokoi H, Matsushime H & Furuichi K (2001). Immunocyte Ca^{2+} influx system mediated by LTRPC2. *Science* **293**, 1327–1330.

Sattler R, Xiong Z, Lu WY, Hafner M, MacDonald JF & Tymianski M (1999). Specific coupling of NMDA receptor activation to nitric oxide neurotoxicity by PSD-95 protein. *Science* **284**, 1845–1848.

Scharenberg AM (2005). TRPM2 and TRPM7: channel/enzyme fusions to generate novel intracellular sensors. *Pflugers Arch* **451**, 220–227.

Smith MA, Herson PS, Lee K, Pinnock RD & Ashford ML (2003). Hydrogen-peroxide-induced toxicity of rat striatal neurones involves activation of a non-selective cation channel. *J Physiol* **547**, 417–425.

Sugawara T, Lewen A, Noshita N, Gasche Y & Chan PH (2002). Effects of global ischemia duration on neuronal, astroglial, oligodendroglial, and microglial reactions in the vulnerable hippocampal CA1 subregion in rats. *J Neurotrauma* **19**, 85–98.

Sun HS, Feng ZP, Miki T, Seino S & French RJ (2006). Enhanced neuronal damage after ischemic insults in mice lacking Kir6.2-containing ATP-sensitive K^+ channels. *J Neurophysiol* **95**, 2590–2601.

Togashi K, Hara Y, Tominaga T, Higashi T, Konishi Y, Mori Y & Tominaga M (2006). TRPM2 activation by cyclic ADP-ribose at body temperature is involved in insulin secretion. *EMBO J* **25**, 1804–1815.

Togashi K, Inada H & Tominaga M (2008). Inhibition of the transient receptor potential cation channel TRPM2 by 2-aminoethoxydiphenyl borate (2-APB). *Br J Pharmacol* **153**, 1324–1330.

Wehage E, Eisfeld J, Heiner I, Jungling E, Zitt C & Luckhoff A (2002). Activation of the cation channel long transient receptor potential channel 2 (LTRPC2) by hydrogen peroxide. A splice variant reveals a mode of activation independent of ADP-ribose. *J Biol Chem* **277**, 23150–23156.

Wollmuth LP & Sakmann B (1998). Different mechanisms of Ca^{2+} transport in NMDA and Ca^{2+}-permeable AMPA glutamate receptor channels. *J Gen Physiol* **112**, 623–636.

Zhang W, Chu X, Tong Q, Cheung JY, Conrad K, Masker K & Miller BA (2003). A novel TRPM2 isoform inhibits calcium influx and susceptibility to cell death. *J Biol Chem* **278**, 16222–16229.

Acknowledgements

The authors would like to thank Dr Stephane Angers for kindly providing the lentivirus packaging vectors used to prepare shRNA. This work was supported by the Canadian Institutes of Health Research Grant MOP15514 (to J.F.M.) and MOP68939 (to M.T.), by the Canadian Stroke Network (J.F.M. and M.T.) and by the Japan-Canada Joint Health Research Program (J.F.M. and Y.M.).